Nanoscale

PAPER

View Article Online
View Journal | View Issue

Cite this: *Nanoscale*, 2015, **7**, 1403

Water dispersible upconverting nanoparticles: effects of surface modification on their luminescence and colloidal stability†

Stefan Wilhelm,[a] Martin Kaiser,[b] Christian Würth,[b] Josef Heiland,[a] Carolina Carrillo-Carrion,[c] Verena Muhr,[a] Otto S. Wolfbeis,[a] Wolfgang J. Parak,[c] Ute Resch-Genger*[b] and Thomas Hirsch*[a]

We present a systematic study on the effect of surface ligands on the luminescence properties and colloidal stability of β-$NaYF_4$:Yb^{3+},Er^{3+} upconversion nanoparticles (UCNPs), comparing nine different surface coatings to render these UCNPs water-dispersible and bioconjugatable. A prerequisite for this study was a large-scale synthetic method that yields ~2 g per batch of monodisperse oleate-capped UCNPs providing identical core particles. These ~23 nm sized UCNPs display an upconversion quantum yield of ~0.35% when dispersed in cyclohexane and excited with a power density of 150 W cm^{-2}, underlining their high quality. A comparison of the colloidal stability and luminescence properties of these UCNPs, subsequently surface modified with ligand exchange or encapsulation protocols, revealed that the ratio of the green (545 nm) and red (658 nm) emission bands determined at a constant excitation power density clearly depends on the surface chemistry. Modifications relying on the deposition of additional (amphiphilic) layer coatings, where the initial oleate coating is retained, show reduced non-radiative quenching by water as compared to UCNPs that are rendered water-dispersible *via* ligand exchange. Moreover, we could demonstrate that the brightness of the upconversion luminescence of the UCNPs is strongly affected by the type of surface modification, *i.e.*, ligand exchange or encapsulation, yet hardly by the chemical nature of the ligand.

Received 9th October 2014,
Accepted 28th November 2014

DOI: 10.1039/c4nr05954a

www.rsc.org/nanoscale

Introduction

Lanthanide-doped upconverting nanoparticles (UCNPs) have gained much attention as a promising class of novel labels and probes in bioanalytical and theranostic applications.[1–4] The sequential absorption of multiple low energy excitation photons by lanthanide ions incorporated into an inorganic host material results in anti-Stokes emission, referred to as upconversion luminescence (UCL).[5] In the case of $NaYF_4$ as the host material and using Yb^{3+} and Er^{3+} as the sensitizer and activator dopant ions, respectively, excitation is typically performed at 980 nm.[6] The advantages of near-infrared (NIR) excitation include: (a) significant minimization of photo-damage to biological specimens, (b) maximization of the penetration depth of the excitation light in biological tissue, and (c) an excellent signal-to-noise ratio along with improved detection sensitivity due to the lack of auto-fluorescence from biological materials.[7–9] Due to the sequential absorption of two or more photons, UCL requires a less intense excitation in comparison to the nonlinear multiphoton absorption of organic dyes or semiconductor nanocrystals.[10] Therefore, excitation can be performed with inexpensive, low-power continuous wave laser diodes. Moreover, and contrary to semiconductor quantum dots, UCNPs do not show intermittent emission (blinking) upon continuous excitation, and emission peak positions are not affected by particle size, making them highly attractive for bioimaging applications.[11] UCNPs can be even used for long-term imaging because they are highly photostable.[12] Additional doping with Gd^{3+} ions results in multimodal nanoparticles beneficial for magnetic resonance imaging or computed tomography applications.[13,14] On the other hand, the nonlinear absorption process renders luminescence quantum

[a]*Institute of Analytical Chemistry, Chemo- and Biosensors, University of Regensburg, 93040 Regensburg, Germany. E-mail: thomas.hirsch@ur.de; Fax: +49-941-943-4064; Tel: +49-941-943-5712*
[b]*BAM Federal Institute for Materials Research and Testing, Division 1.10 Biophotonics, Richard-Willstätter-Str. 11, 12489 Berlin, Germany. E-mail: ute.resch@bam.de; Fax: +49-30-8104-1157; Tel: +49-30-8104-1134*
[c]*FB Physics, AG Biophotonics, Philipps University of Marburg, Renthof 7, 35037 Marburg, Germany*

†Electronic supplementary information (ESI) available: Protocols of the synthesis of OA-coated UCNPs and their surface modifications, quantification of the UCNP composition, quantification of the UCNP concentration, and quantification of OA surface ligands. See DOI: 10.1039/c4nr05954a

yields dependent on the power density of the excitation light source. Besides a preferably high upconversion efficiency under application-relevant conditions, which requires synthetic strategies yielding high quality spherical and monodisperse UCNPs of pure crystallinity and exact stoichiometric composition, there are several other requirements that must be fulfilled by UCNPs for use in bioanalytical and biological applications. These include water dispersibility, high colloidal stability, the possibility of subsequent (bio)functionalization, and good bio-compatibility.[15] These require post synthetic treatments and the introduction of hydrophilic and bioconjugatable ligands,[16] as current advanced synthetic strategies for the preparation of high-quality lanthanide-doped hexagonal (= β-phase) $NaYF_4$ UCNPs are based on oil-phase methods, yielding hydrophobic UCNPs.[15,17,18]

The luminescence properties and especially the upconversion efficiency of UCNP are very sensitive to variations in the surface area-to-volume ratio, crystal structure, and lanthanide doping concentration as well as to the ligand and surrounding medium.[19] For example, the UCL of Yb^{3+},Er^{3+}-doped $NaYF_4$ nanocrystals with diameters of 6–45 nm (cubic or hexagonal phases) display an increasing red-to-green luminescence intensity ratio with decreasing particle size,[20] and surface-bound compounds (*e.g.*, C–H, O–H vibrational modes of stabilizing ligands) or hydroxyl groups in aqueous media can act as luminescence quenchers.[21–24] Hence, the rational design of UCNPs with bright emission in water even at low excitation power densities requires a comprehensive understanding of the processes inducing luminescence quenching, which has not yet been really achieved. The derivation of a detailed picture of all parameters affecting the luminescence of UCNPs requires systematic studies of identical particles (size, size distribution, and material composition) functionalized with different ligands and validated spectroscopic methods.[25]

This encouraged us to study the luminescence behavior and colloidal stability of UCNPs of identical core, subsequently surface modified with nine typical ligands and coatings, rendering these particles water dispersible. This included exchange of oleate for hydrophilic ligands, encapsulation with an amphiphilic polymer, and silica coating. With this study, we were able to expand the complex picture of UCNP luminescence.

Results and discussion

Large-scale synthesis of oleate-coated UCNPs

Pure hexagonal-phase $NaYF_4$ nanocrystals doped with lanthanide ions were prepared in mixtures of oleic acid and 1-octadecene at 300 °C according to a method first reported by Li *et al.*[26] This protocol is now being widely used,[27–30] but has still certain disadvantages: these include (1) the need for careful stabilization of temperature (300 °C for 1 h), and (2) the relatively small scale (only ~100 mg of UCNP can be obtained in a single batch). However, each batch will yield particles that are slightly different in terms of size, shape, elemental composition and, hence, UCL.[21,23] Thus, for really systematic studies, a method for synthesis is favored (and needed) that yields large amounts of identical UCNPs with a minimum variation in size and composition in one batch.

The method presented here has several attractive features: (1) it yields β-UCNPs in a simple single-batch reaction due to the proper control of the reaction conditions; (2) the process can be monitored with bare eyes *via* the strong luminescence of the final product formed; and (3) when using our optimized protocol, a temperature stabilization at exactly 300 °C is not mandatory since the reaction mixture is heated to reflux (~320 °C; Fig. 1). A diagram that reveals the progression of the temperature during synthesis is displayed in Fig. 1a. A timer was started when the reaction mixture had reached 300 °C (Fig. S1†). The onset of the crystallization of the $NaYF_4$:Yb^{3+}, Er^{3+} UCNPs is characterized by the formation of small (~5 nm in diameter) cubic-phase UCNPs as the first products. This was verified by X-ray powder diffraction (XRD; Fig. 1b) and transmission electron microscopy (TEM; Fig. 1d). Subsequently, the α-UCNPs are transformed into β-UCNPs at temperatures >300 °C.[6] We find that this step can be well monitored with bare eyes by illuminating the reaction vessel with a 980 nm cw diode laser (~10 W cm^{-2}) in order to excite the UCL.[31] The formation of the β-UCNPs is accompanied by the appearance of green luminescence, which begins to appear after ~22 min at >300 °C (Fig. 1c). XRD and TEM studies of a sample taken at this time verify the presence of smaller (~5 nm) α-UCNPs and larger (~16 nm) β-UCNPs. When using an even higher laser power density, it is expected that the upconversion luminescence may be observed earlier and there-

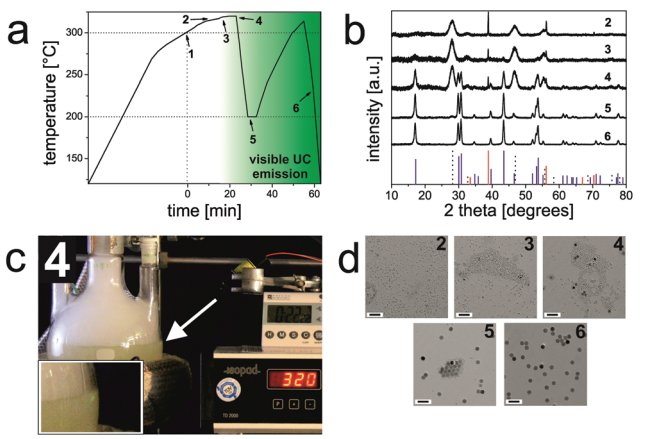

Fig. 1 Large-scale synthesis of monodisperse β-$NaYF_4$:Yb^{3+},Er^{3+} UCNPs. (a) Diagram showing the temperature evolution as a function of the reaction time. The timer was started when the temperature of the reaction mixture had reached 300 °C (1). Samples of the reaction mixture were characterized by XRD (b) and TEM (d) after 10 min (2), 15 min (3), 22 min (4), 27 min (5), and 60 min (6). (c) Image of the synthesis setup illuminated with a 980 nm cw laser (~10 W cm^{-2}). Green upconversion luminescence (inset) was detectable for the first time after ~22 minutes (4). XRD reference patterns: cubic NaF (ICDD PDF #36-1455): red solid lines; cubic $NaYF_4$ (ICDD PDF #77-2042): black dotted lines; hexagonal $NaYF_4$ (ICDD PDF #16-0334): blue solid lines. Scale bars indicate 60 nm.

fore the resulting β-UCNPs will be smaller. Once the UCL becomes visible, the reaction mixture is cooled to 200 °C to prevent further growth of the β-UCNPs and a broadening of the particle size distribution.[32] The TEM image of the UCNP obtained at 200 °C displays a bimodal particle distribution, *i.e.*, one fraction of larger β-UCNPs and a second fraction of smaller α-UCNPs. This was further verified by XRD measurements (Fig. 1). In order to yield pure β-UCNPs, an additional heating step (~5 minutes, >300 °C) was applied. This resulted in the disintegration of the α-UCNPs and the growth of the β-UCNPs as confirmed by TEM and XRD studies (Fig. 1).

It is known that the efficiency of UCL is about one order of magnitude higher for large lanthanide-doped hexagonal $NaYF_4$ particles compared to the respective cubic phase materials.[33] However, the efficiency of UCL decreases rapidly as the surface-to-volume ratio increases. This is ascribed to non-radiative deactivation of excited state lanthanide ions by surface defects, surface-bound ligands and, depending on the surroundings of the UCNPs, also by solvent molecules with high vibrational energy modes.[23,34–36] Thus, based on the strong UCL observed, we presume an even higher difference in UCL efficiency between small α-UCNPs and large β-UCNPs formed within a few minutes.

This preparation procedure enables to scale up the synthesis of monodisperse β-UCNPs by a factor of 20 in comparison to the protocol of Li *et al.*,[26] and we were able to obtain ~2 g of oleate-coated (OA) β-$NaYF_4$:Yb^{3+},Er^{3+} UCNPs of purely hexagonal crystal structure in a single batch for subsequent systematic functionalization studies with identical UCNPs.

Analytical characterization of UCNPs

TEM images of OA-coated UCNPs displayed in Fig. 2 demonstrate their narrow size distribution (average core diameter 22.7 ± 0.7 nm) and a uniform, roughly spherical shape. The hydrophobic capping is not detectable in TEM. The variation in size (expressed as standard deviation) is as low as ~3%. The inset of Fig. 2a shows the lattice fringes with a spacing of ~0.5 nm for a single UCNP. XRD measurements (Fig. 2b) verify the purely hexagonal crystal structure of $NaYF_4$:Yb^{3+},Er^{3+} UCNPs as compared to the XRD pattern of standard β-$NaYF_4$:Yb^{3+},Er^{3+} (The International Centre for Diffraction Data, Powder Diffraction File; ICDD PDF #16-0334). The diameter of the crystalline domains in the UCNPs derived from the XRD experiments using Scherrer's equation is 23 ± 1.3 nm. This is in good agreement with the diameter obtained from the analysis of the TEM images.[37]

Dynamic light scattering (DLS) experiments with OA-coated UCNPs using an intensity-weighted size distribution model revealed a solvodynamic diameter of 29 ± 3 nm with a polydispersity index (PdI) of 0.19 in cyclohexane (Fig. 3a). The rare-earth ion content of β-$NaYF_4$:Yb^{3+},Er^{3+} UCNPs was determined using inductively coupled plasma optical emission spectroscopy (ICP-OES). The fractions of 78.4 ± 0.1 mol% of Y^{3+}, 19.3 ± 0.1 mol% of Yb^{3+}, and 2.3 ± 0.1 mol% of Er^{3+}, respectively, are in good agreement with the concentrations calculated from the amounts of lanthanide ions applied in the synthesis (Table S1†). This underlines the excellent quality of our OA-coated β-$NaYF_4$:Yb^{3+},Er^{3+} UCNPs in terms of size distribution, shape uniformity, elemental composition, and crystalline phase.

To determine the initial ligand density/concentration per UCNP, we performed thermal gravimetric analysis (TGA) experiments over the temperature range of 35–600 °C under an atmosphere of nitrogen at a heating rate of 10 °C min^{-1} (Fig. 3b). This yielded a mass loss of ~9.1% for the initially OA-coated UCNPs. From the results of the TGA experiments, we calculated the number of OA ligands per UCNP (22.7 nm core diameter) to be ~5.7×10^3. This equals a ligand surface coverage of ~70% (ESI†).

Luminescence properties

The OA-coated β-$NaYF_4$:Yb^{3+},Er^{3+} UCNPs (22.7 nm core diameter) dispersed in cyclohexane show a luminescence quantum yield (QY) of ~0.35% at a power density of 150 W cm^{-2} as determined absolutely with the integration sphere setup described earlier.[38] This exceeds the QY of ~0.1% reported by Boyer *et al.* for OA-coated β-$NaYF_4$:Yb^{3+},Er^{3+} UCNPs dispersed in hexane with a core diameter of 30 nm assuming that the upconversion QY is mainly governed by the ratio of surface area to volume and, hence, the number of surface defects.[23,35–37] Possibly, our improved protocol for UCNP synthesis yields UCNPs with a reduced number of surface defects.

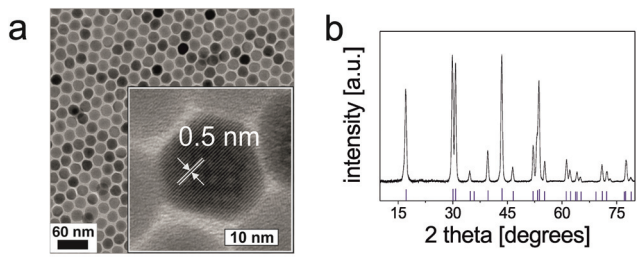

Fig. 2 Characterization of UCNPs. (a) TEM image of OA-coated β-$NaYF_4$:Yb^{3+},Er^{3+} UCNPs. The inset displays lattice fringes of a single UCNP with a lattice spacing of ~0.5 nm. (b) The UCNPs produced by our method exhibit purely hexagonal (β-phase) crystal structure of $NaYF_4$ as compared to the XRD standard pattern (ICDD PDF #16-0334).

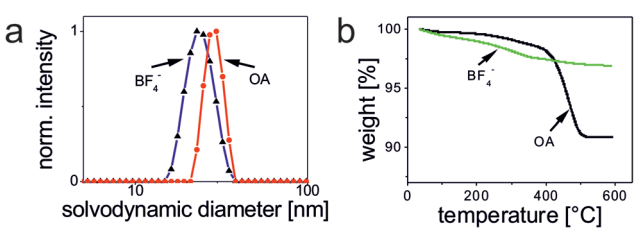

Fig. 3 (a) The solvodynamic diameter (intensity-weighted distribution) of OA-coated UCNPs in cyclohexane is 29 nm (PdI 0.189), and 24 nm (PdI 0.089) for BF_4^--coated UCNPs (BF_4^-) in DMF. (b) TGA experiments quantifying the relative mass loss of OA-coated and BF_4^--coated UCNPs as ~9.1% and ~3.1%, respectively.

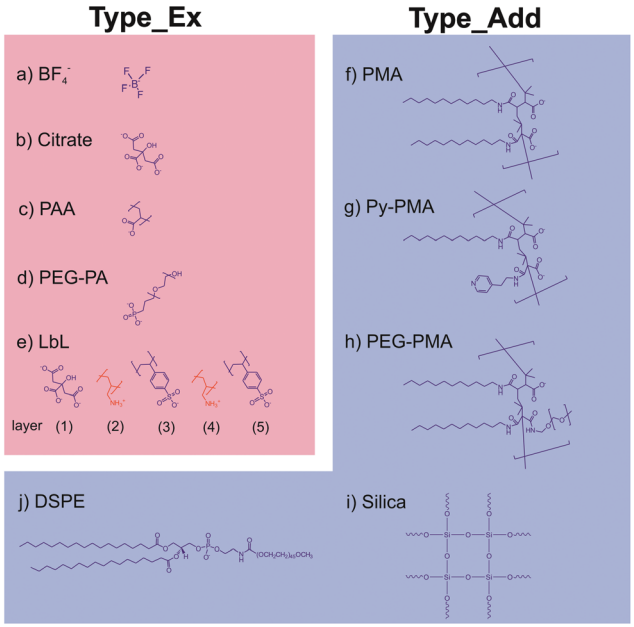

Scheme 1 Overview of general strategies for surface modification of oleate-coated UCNPs of the $NaYF_4$:Yb^{3+},Er^{3+} type. The modifications can be classified into two categories: (a)–(e) ligand exchange methods (Type_Ex); (f)–(j) addition of an amphiphilic layer or silica coating (Type_Add). Note: the oleate layer is still present for Type_Add modifications. Examples of Type_Ex modifications include coating with: (a) tetrafluoroborate (BF_4^-); (b) trisodium citrate (citrate); (c) poly(acrylic acid sodium salt) (PAA); (d) poly(ethylene-oxide)-10-OH with a terminal phosphate ester (PEG-PA); (e) layer-by-layer coating with poly(sodium 4-styrenesulfonate) (PSS) and poly(allylamine hydrochloride) (PAH) (LbL) on an initial citrate layer. Examples of Type_Add modifications are coating with: (f) poly(isobutylene-*alt*-maleic anhydride) modified with dodecylamine (PMA); (g) the same as (f) but with a further modification with 4-(aminomethyl)pyridine (Py-PMA); (h) the same as (f) but with further modification with α-methoxy-ω-amino poly(ethylene glycol)-1200 (PEG-PMA); (i) silica coating with a shell thickness of ~5 nm (silica); (j) 1,2-distearoyl-*sn*-glycero-3-phospho-ethanolamine-*N*-[methoxy-(poly-ethylene glycol)-2000] (ammonium salt) (DSPE).

Surface modifications

Subsequently, we modified the hydrophobic surface of our UCNPs with different commonly used strategies for surface modification, which are displayed in Scheme 1. These procedures included strategies involving the deposition of either an additional amphiphilic or silica coating while maintaining the original hydrophobic capping on the UCNPs (Type_Add). For this type of surface modification, which utilizes an additional shell covering the OA layer, we used amphiphilic molecules (DSPE), amphiphilic polymers (PMA, Py-PMA, PEG-PMA) or a silica shell (shell thickness ~5 nm). The second strategy involves the complete exchange of the original OA ligands by a hydrophilic ligand (Type_Ex); here BF_4^-, the strongly coordinating citrate anion, PEG-type ligands, and polymeric ligands were investigated. A generalized ligand exchange strategy has been reported by Dong *et al.*[39] using nitrosonium tetrafluoroborate ($NOBF_4$) to replace the original OA ligands attached to the UCNPs surface. This procedure enables the phase transfer of initially hydrophobic UCNPs to polar, hydrophilic media such as *N*,*N*-dimethylformamide (DMF), which is very attractive for their biophysical, bioanalytical and imaging applications.[40–44]

Analytical characterization

The TEM images of all surface-modified UCNPs are summarized in Fig. 4. Table 1 contains the results of the DLS and zeta-potential measurements. The latter underlines that stable, optically transparent colloids resulted from all nine surface modifications (*i.e.*, both general strategies) in double-distilled (dd) water at pH 7. The DLS measurements (Table 1) demonstrate that in the case of the encapsulation strategy, where an additional shell is formed on the original hydrophobic coating, the hydrodynamic diameter is only slightly larger than the diameter of the inorganic core (revealed from TEM). This indicates that the monodispersity of the UCNPs was

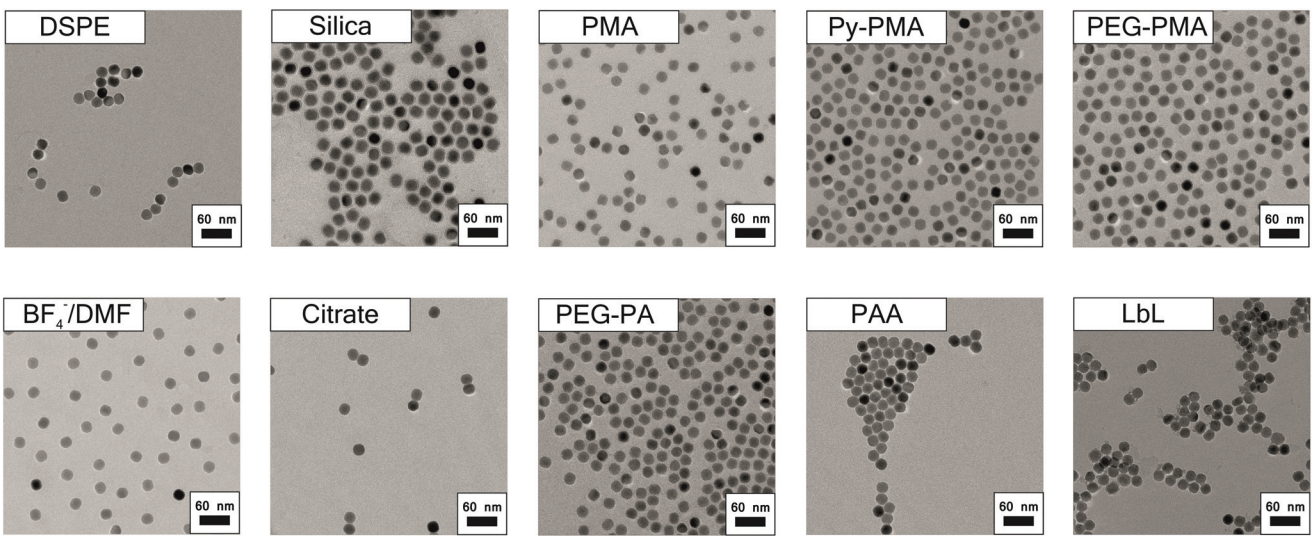

Fig. 4 TEM images of Type_Add (first row) and Type_Ex (second row) surface-modified UCNPs. The surface modification protocols led to colloidally stable UCNPs dispersed in water without any tendency to aggregate. Scale bars indicate 60 nm.

Table 1 Summary of the results of the DLS and zeta-potential measurements

	Ligand[a]	Hydrodynamic diameter[b] [nm]	PdI[c]	Zeta potential[d] [mV]
Type_Add	PMA	34	0.176	−53
	PEG-PMA	35	0.147	−52
	Py-PMA	39	0.091	−51
	Silica	42	0.223	−32
	DSPE	53	0.098	−9
Type_Ex	PAA	37	0.199	−36
	LbL	33	0.182	−34
	Citrate	24	0.025	−25
	PEG-PA	77	0.181	18

[a] For full names of ligands see Scheme 1. [b] DLS results based on an intensity-weighed size distribution model. [c] Polydispersity index. [d] Zeta potential in dd water at pH 7 (UCNP concentration 10 mg mL^{-1}).

maintained during the phase transfer from organic to aqueous solution, thereby excluding the formation of agglomerates. The increase in size upon the formation of the PMA shell is in good agreement with previous data.[45] Our UCNPs surface-modified with the Type_Add strategy are suitable for biophysical, bioanalytical, and imaging applications.[46–49]

Analytical characterization of the UCNP surface modified *via* ligand exchange revealed complete removal of the OA ligand as exemplarily shown for BF_4^--coated UCNPs using TGA. Here, a relative mass loss of ~3.1% indicates the successful exchange of OA for smaller weight BF_4^-. The TEM image of these BF_4^--coated UCNPs is shown in Fig. 4. These particles exhibit a solvodynamic diameter of 24 nm (PdI 0.089) as revealed by DLS experiments in DMF (Fig. 3a). The hydrodynamic diameter of the UCNPs of Type_Ex (24–77 nm) cover the same range as UCNPs of Type_Add (34–53 nm). Additionally, we could demonstrate that hydrophilic BF_4^--stabilized UCNPs can be covered with polymers (PAA) or small molecules (citrate and PEG-PA) using a sequential coating step. The BF_4^-- and citrate-coated UCNPs have smaller solvo-/hydrodynamic diameters compared to the Type_Add UCNPs. This confirms that these UCNPs are capped only by a ligand monolayer and thus show the smallest possible effective size. Particles modified by this (Type_Ex) strategy offer the ability to minimize the distance of a receptor or a probe to the luminescent UCNP, enabling a more efficient fluorescence resonance energy transfer than the UCNP obtained with the encapsulation (Type_Add) approach. Citrate-coated UCNPs may be further modified *via* sequential deposition of positively and negatively charged polymers (PAH and PSS) based on a layer-by-layer (LbL) strategy. In the case of PEG-PA, formation of agglomerates is likely to occur, as the resulting larger hydrodynamic diameters cannot be explained solely by the size of single UCNPs.

Luminescence properties of surface-modified UCNPs

UCNPs based on β-$NaYF_4$:Yb^{3+},Er^{3+} display two dominant anti-Stokes-type emission peaks at 545 nm and 658 nm upon 980 nm cw laser excitation with a full width at half maximum (FWHM) of ~16 nm and ~19 nm, respectively (Fig. 5). The QYs of representative surface-modified UCPNs, here DSPE-modified UCNPs (Type_Add) and citrate-modified UCNPs (Type_Ex) in aqueous dispersions, are approximately two times lower than those in cyclohexane at an excitation power density of 150 W cm^{-2}. This demonstrates the quenching effect caused by water.[37] Moreover, we observed a change in the relative intensity ratios of the upconversion emission bands in water dispersion. This follows from a comparison of the luminescence spectra of all surface-modified UCNPs shown in Fig. 5, which were all acquired under identical measurement conditions (excitation power density of 15 W cm^{-2}) and normalized to the intensity at 658 nm. Interestingly, as can be seen in Fig. 5, our two phase transfer strategies Type_Add and Type_Ex lead to particles that are clearly distinguishable by the different intensity ratios ($I_{g/r}$) of the upconversion emission maxima at 545 nm (green; g) and at 658 nm (red; r). We found the ratio $I_{g/r}$ for Type_Add and Type_Ex surface-modified UCNPs to be ~0.7 and ~0.5, respectively (Fig. 5b and c). This is ascribed to the presence of hydrophobic OA ligands in the former case, which cover ~70% of the UCNP surface and hinder at least partly the direct access of water molecules to the particle surface. Therefore, if green luminescence is to be used in any applications, surface modifications of Type_Add are advised.

Then we compared the spectra of water-dispersible UCNPs to those of the initially prepared particles with OA coating dispersed in cyclohexane (Fig. 5a). This comparison clearly demonstrates the considerable effect of water on the relative intensities of both emission bands. The intensity of the emission at 545 nm drops by a factor of ~3, regardless of the type of surface engineering performed to achieve phase transfer.

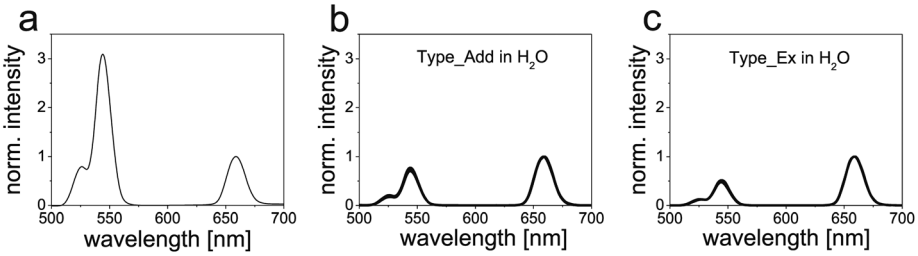

Fig. 5 Normalized upconversion luminescence spectra of UCNPs. The spectra were acquired upon 980 nm cw laser excitation with a power density of 15 W cm^{-2} and are normalized at 658 nm. (a) Spectra of OA-coated UCNPs in cyclohexane ($I_{g/r}$ ~ 3); (b) five spectra of Type_Add surface-modified UCNPs dispersed in water ($I_{g/r}$ ~ 0.7); (c) four spectra of Type_Ex surface-modified UCNPs dispersed in water ($I_{g/r}$ ~ 0.5).

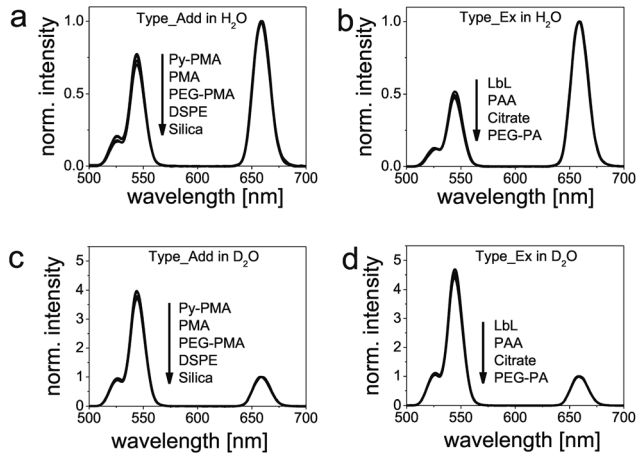

Fig. 6 Normalized upconversion luminescence spectra of Type_Add and Type_Ex surface-modified UCNPs. Spectra were acquired upon 980 nm cw laser excitation (15 W cm^{-2}) and normalized at 658 nm. (a) Type_Add surface-modified UCNPs dispersed in water ($I_{g/r} \sim 0.7$); (b) Type_Ex surface-modified UCNPs dispersed in water ($I_{g/r} \sim 0.5$); (c) Type_Add surface-modified UCNPs dispersed in D_2O ($I_{g/r} \sim 4$); (d) Type_Ex surface-modified UCNPs dispersed in D_2O ($I_{g/r} \sim 4.7$).

To gain further insight into the luminescence deactivation mechanisms of UCNPs, we compared the relative luminescence intensities in H_2O and D_2O. D_2O can prevent luminescence quenching of excited lanthanide ions by high-energy O–H vibrational modes.[37] The corresponding normalized upconversion emission spectra are displayed in Fig. 6. As expected, an increase by a factor of ~6 $I_{g/r}$ and ~9 $I_{g/r}$ is found for D_2O solutions of UCNPs surface-modified with Type_Add and Type_Ex strategies, respectively. Also in D_2O, both types of surface modifications can be easily distinguished, with Type_Ex modifications exhibiting a higher $I_{g/r}$ ratio compared to particles obtained with Type_Add modifications. We attribute this effect to the luminescence quenching caused by the C–H vibrational modes of OA ligands and the amphiphilic coatings.

Our results have two major implications: if surface-modified UCNPs are applied for self-referenced and quantitative sensing such as temperature sensing or the sensing of chemical species, UCNPs with Type_Add modifications exhibit a wider dynamic range of $I_{g/r}$ (provided that the excitation power density is constant). This is beneficial for sensing schemes that rely on inner filter effects where UCNPs basically act as a type of nanolamps.[50–53] UCNPs with modifications of Type_Ex, in turn, are better suited for designing sensors utilizing fluorescence resonance energy transfer (FRET) since the distance between donors (lanthanide ions) and acceptors (*e.g.*, stimuli-responsive dyes) can be minimized. It is expected that a decrease in the particle diameter will further enlarge the luminescence intensity ratio ($I_{g/r}$) of particles prepared by these two strategies for surface modification. For all applications which do not rely on a FRET, the growth of an additional shell of undoped $NaYF_4$ or other materials lacking low energy phonons will prevent non-radiative relaxation processes by solvent molecules and minimize the influence of surface ligands on the upconversion luminescence.[34,54–56]

Conclusions

In summary, following an improved and upscaled protocol for the synthesis of high quality β-$NaYF_4$:Yb^{3+},Er^{3+} UCNPs, we prepared nine differently surface modified UCNPs from the same core material using encapsulation and ligand exchange strategies. In each case, water-dispersible β-UCNPs with excellent colloidal stability suitable for subsequent functionalization and bioconjugation were obtained. The brightness of these UCNPs in water is significantly reduced compared to the hydrophobic original UCNPs. This is attributed to the non-radiative decay of the electronically excited states of the dopant lanthanide ions caused by surface ligands and water molecules. The various surface chemistries can be distinguished by the intensity ratios of the red and green upconversion emission bands ($I_{g/r}$), enabling the classification of both types of surface modifications. All modifications consisting of an additional layer on top of the original oleate ligand show a brighter green luminescence compared to the intensity of the red emission, regardless of the type of ligand used, in contrast to all surface modifications performed by a ligand exchange. Our results suggest that Type_Add modifications provide a wider dynamic range of $I_{g/r}$ favorable, *e.g.*, for sensing schemes that rely on inner filter effects. UCNPs with modifications of Type_Ex seem to be better suited for the design of sensors utilizing fluorescence resonance energy transfer. This is currently being studied for differently sized UCNPs.

Methods

Materials

Yttrium(III) chloride hexahydrate (99.99%) and ytterbium(III) chloride hexahydrate (99.9%) were purchased from Treibacher Industrie AG (Althofen, Austria). Ammonium fluoride (ACS reagent ≥98.0%), erbium(III) chloride hexahydrate (99.99%), sodium hydroxide (reagent grade, ≥98.0%), Igepal® CO-520, tetraethyl orthosilicate (TEOS), nitrosyl tetrafluoroborate (95%), poly(isobutylene-*alt*-maleic anhydride) (PMA) (average $M_w \sim 6$ kDa), dodecylamine (98%), 4-(aminomethyl)pyridine (98%), *N*-(3-dimethylaminopropyl)-*N*′-ethylcarbodiimide hydrochloride (EDC), poly(acrylic acid sodium salt) (PAA) (average $M_w \sim 2.1$ kDa), deuterium oxide (99.9 atom% D), poly(allylamine hydrochloride) (PAH) (average $M_w \sim 15$ kDa), boric acid (99.999%), and poly(sodium-4-styrenesulfonate) (PSS) (average $M_w \sim 15$ kDa) were purchased from Sigma-Aldrich (Steinheim, Germany). α-Methoxy-ω-amino-poly(ethylene-glycol)-1200 (CH_3O-PEG-NH_2) (average $M_w \sim 1.2$ kDa) was obtained from Rapp Polymere (Tuebingen, Germany). Oleic acid (technical grade, 90%) and 1-octadecene (technical grade, 90%) were from Alfa Aesar (Karlsruhe, Germany). DSPE-mPEG(2000) (1,2 distearoyl-*sn*-glycero-3-phosphoethanolamine-*N*-[methoxy(poly

ethylene-glycol)-2000] (ammonium salt)) was purchased from Avanti Polar Lipids (Alabaster, Alabama). An ammonia solution (32%), tri-sodium citrate dihydrate, sulfuric acid (95–97%), and nitric acid (70%) were purchased from Merck (Darmstadt, Germany). PEO-10-OH-terminated phosphonic acid (PEG-PA) was from Specific Polymers (Castries, France). *N*,*N*-Dimethylformamide (DMF) (99.5%), chloroform (99%), tetrahydrofuran (THF) (99.8%), and cyclohexane (99.5%) were from Acros Organics (Geel, Belgium). All other reagents and organic solvents were of the highest grade available. Unless otherwise noted, all chemicals were used as received without any further purification.

Instruments

Transmission electron microscopy (TEM) was performed using a Philips CM12 microscope operating at 120 kV (Hillsboro, Oregon). The size distributions of the UCNPs were evaluated from the TEM images using ImageJ software (http://rsbweb.nih.gov/ij/). We used the Zetasizer Nano ZS from Malvern (Herrenberg, Germany) for dynamic light scattering (DLS) experiments with intensity-weighed distribution mode. X-ray powder diffraction (XRD) patterns with a resolution of 0.005° (2θ) were collected using a Huber Guinier G670 diffractometer (Rinsting, Germany) with a Cu source (Kα radiation, λ = 1.54060 Å) operating at 40 kV and 30 mA. All standard XRD reference patterns are referred to the database of the International Centre for Diffraction Data (ICDD). A Spectro Flame-EOP (Kleve, Germany) inductively coupled plasma optical emission spectrometer (ICP-OES) was used for the determination of the amount of rare-earth ions in the UCNPs. All centrifugation steps were carried out using a Hettich Universal 320 centrifuge (Tuttlingen, Germany). A Sonorex Digitech DT255H ultrasonic bath from Bandelin (Berlin, Germany) was used. UCL spectra were recorded at room temperature with a dye-calibrated luminescence spectrometer (LS 50 B) from Perkin Elmer (Waltham, Massachusetts) modified with a 980 nm cw laser module (120 mW, 15 W cm^{-2}) from Roithner (Vienna, Austria) for upconversion photo-excitation.[57] A thermal gravimetric analysis (TGA) was performed using a Perkin-Elmer TGA 7 set-up (Waltham, Massachusetts). The synthesis was monitored using a 980 nm cw laser module (200 mW, ~10 W cm^{-2}) from Roithner (Vienna, Austria) for upconversion photo-excitation. The absolute determination of upconversion quantum yields was performed with a calibrated integrating sphere setup equipped with an 8 W 980 nm laser diode at precisely controlled excitation power densities.[41] For QY determination the UCL intensity was integrated in the spectral range of 300–900 nm.

Acknowledgements

The authors thank Prof. Reinhard Rachel for his support with the transmission electron microscopy, Nadja Leibl for assistance with the particle synthesis, Dr Rainer Müller for the TGA measurements, and Joachim Rewitzer for the ICP-OES measurements. Furthermore, Dr Richard Weihrich is acknowledged for providing the XRD measurement device and Prof. Markus Haase for ongoing discussions on UCNPs. This work was part of a project of the German Research Foundation (DFG; WO 669/12-1). MK gratefully acknowledges financial support from the Federal Ministry of Economics and Technology (BMWI-14/09; MNPQ program) and CW acknowledges the Federal Ministry of Economics and Technology (BMWI-11/12; MNPQ program). Part of this project was supported by the German Research Foundation (DFG; project GRK 1782 to WJP). CCC is grateful for a postdoctoral fellowship from the Alexander von Humboldt Foundation.

Notes and references

1 J. Zhou, Z. Liu and F. Li, *Chem. Soc. Rev.*, 2012, **41**, 1323–1349.
2 F. Zhang, G. B. Braun, Y. Shi, Y. Zhang, X. Sun, N. O. Reich, D. Zhao and G. Stucky, *J. Am. Chem. Soc.*, 2010, **132**, 2850–2851.
3 L. Xiong, Z. Chen, Q. Tian, T. Cao, C. Xu and F. Li, *Anal. Chem.*, 2009, **81**, 8687–8694.
4 R. Kumar, M. Nyk, T. Y. Ohulchanskyy, C. A. Flask and P. N. Prasad, *Adv. Funct. Mater.*, 2009, **19**, 853–859.
5 F. Auzel, *Chem. Rev.*, 2004, **104**, 139–174.
6 M. Haase and H. Schäfer, *Angew. Chem., Int. Ed.*, 2011, **50**, 5808–5829.
7 Q. Zhan, J. Qian, H. Liang, G. Somesfalean, D. Wang, S. He, Z. Zhang and S. Andersson-Engels, *ACS Nano*, 2011, **5**, 3744–3757.
8 J. Pichaandi, J.-C. Boyer, K. R. Delaney and F. C. J. M. van Veggel, *J. Phys. Chem. C*, 2011, **115**, 19054–19064.
9 Y. Yang, Q. Shao, R. Deng, C. Wang, X. Teng, K. Cheng, Z. Cheng, L. Huang, Z. Liu, X. Liu and B. Xing, *Angew. Chem., Int. Ed.*, 2012, **51**, 3125–3129.
10 X. Wang, D. E. Achatz, C. Hupf, M. Sperber, J. Wegener, S. Bange, J. M. Lupton and O. S. Wolfbeis, *Sens. Actuators, B*, 2013, **188**, 257–262.
11 S. Wu, G. Han, D. J. Milliron, S. Aloni, V. Altoe, D. V. Talapin, B. E. Cohen and P. J. Schuck, *Proc. Natl. Acad. Sci. U. S. A.*, 2009, **106**, 10917–10921.
12 D. J. Gargas, E. M. Chan, A. D. Ostrowski, S. Aloni, M. V. P. Altoe, E. S. Barnard, B. Sanii, J. J. Urban, D. J. Milliron, B. E. Cohen and P. J. Schuck, *Nat. Nanotechnol.*, 2014, **9**, 300–305.
13 Y. Liu, D. Tu, H. Zhu and X. Chen, *Chem. Soc. Rev.*, 2013, **42**, 6924–6958.
14 G. Chen, H. Qiu, P. N. Prasad and X. Chen, *Chem. Rev.*, 2014, **114**, 5161–5214.
15 X. Ye, J. E. Collins, Y. Kang, J. Chen, D. T. N. Chen, A. G. Yodh and C. B. Murray, *Proc. Natl. Acad. Sci. U. S. A.*, 2010, **107**, 22430–22435.
16 R. Mout, D. F. Moyano, S. Rana and V. M. Rotello, *Chem. Soc. Rev.*, 2012, **41**, 2539–2544.

17 F. Wang, Y. Han, C. S. Lim, Y. Lu, J. Wang, J. Xu, H. Chen, C. Zhang, M. Hong and X. Liu, *Nature*, 2010, **463**, 1061–1065.
18 S. Gai, C. Li, P. Yang and J. Lin, *Chem. Rev.*, 2014, **114**, 2343–2389.
19 C. T. Xu, Q. Zhan, H. Liu, G. Somesfalean, J. Qian, S. He and S. Andersson-Engels, *Laser Photonics Rev.*, 2013, **7**, 663–697.
20 J. Zhao, Z. Lu, Y. Yin, C. McRae, J. A. Piper, J. M. Dawes, D. Jin and E. M. Goldys, *Nanoscale*, 2013, **5**, 944–952.
21 J.-C. G. Bünzli and C. Piguet, *Chem. Soc. Rev.*, 2005, **34**, 1048–1077.
22 F. Wang, J. Wang and X. Liu, *Angew. Chem., Int. Ed.*, 2010, **49**, 7456–7460.
23 C. Bischof, J. Wahsner, J. Scholten, S. Trosien and M. Seitz, *J. Am. Chem. Soc.*, 2010, **132**, 14334–14335.
24 H. Liu, C. T. Xu, D. Lindgren, H. Xie, D. Thomas, C. Gundlach and S. Andersson-Engels, *Nanoscale*, 2013, **5**, 4770–4775.
25 F. C. J. M. van Veggel, C. Dong, N. J. J. Johnson and J. Pichaandi, *Nanoscale*, 2012, **4**, 7309–7321.
26 Z. Li, Y. Zhang and S. Jiang, *Adv. Mater.*, 2008, **20**, 4765–4769.
27 C. Liu, Y. Hou and M. Gao, *Adv. Mater.*, 2014, **26**, 6922–6932.
28 Y. Hou, R. Qiao, F. Fang, X. Wang, C. Dong, K. Liu, C. Liu, Z. Liu, H. Lei, F. Wang and M. Gao, *ACS Nano*, 2013, **7**, 330–338.
29 Y.-H. Chien, Y.-L. Chou, S.-W. Wang, S.-T. Hung, M.-C. Liau, Y.-J. Chao, C.-H. Su and C.-S. Yeh, *ACS Nano*, 2013, **7**, 8516–8528.
30 S. Wilhelm, T. Hirsch, W. M. Patterson, E. Scheucher, T. Mayr and O. S. Wolfbeis, *Theranostics*, 2013, **3**, 239–248.
31 J. D. Suter, N. J. Pekas, M. T. Berry and P. S. May, *J. Phys. Chem. C*, 2014, **118**, 13238–13247.
32 B. Voss and M. Haase, *ACS Nano*, 2013, **7**, 11242–11254.
33 K. W. Krämer, D. Biner, G. Frei, H. U. Güdel, M. P. Hehlen and S. R. Lüthi, *Chem. Mater.*, 2004, **16**, 1244–1251.
34 J.-C. Boyer and F. C. J. M. van Veggel, *Nanoscale*, 2010, **2**, 1417–1419.
35 S. Wu, Y. Ning, J. Chang and S. Zhang, *J. Lumin.*, 2013, **143**, 492–497.
36 J.-C. Boyer, M.-P. Manseau, J. I. Murray and F. C. J. M. van Veggel, *Langmuir*, 2010, **26**, 1157–1164.
37 J.-C. Boyer, F. Vetrone, L. A. Cuccia and J. A. Capobianco, *J. Am. Chem. Soc.*, 2006, **128**, 7444–7445.
38 C. Würth, J. Pauli, C. Lochmann, M. Spieles and U. Resch-Genger, *Anal. Chem.*, 2012, **84**, 1345–1352.
39 A. Dong, X. Ye, J. Chen, Y. Kang, T. Gordon, J. M. Kikkawa and C. B. Murray, *J. Am. Chem. Soc.*, 2011, **133**, 998–1006.
40 L.-L. Li, R. Zhang, L. Yin, K. Zheng, W. Qin, P. R. Selvin and Y. Lu, *Angew. Chem., Int. Ed.*, 2012, **25**, 6225–6229.
41 T. Pellegrino, L. Manna, S. Kudera, T. Liedl, D. Koktysh, A. L. Rogach, S. Keller, J. Rädler, G. Natile and W. J. Parak, *Nano Lett.*, 2004, **4**, 703–707.
42 R. A. Sperling, T. Pellegrino, J. K. Li, W. H. Chang and W. J. Parak, *Adv. Funct. Mater.*, 2006, **16**, 943–948.
43 R. A. Sperling, T. Liedl, S. Duhr, S. Kudera, M. Zanella, C.-A. J. Lin, W. H. Chang, D. Braun and W. J. Parak, *J. Phys. Chem. C*, 2007, **111**, 11552–11559.
44 S. Jiang, K. Y. Win, S. Liu, C. P. Teng, Y. Zheng and M.-Y. Han, *Nanoscale*, 2013, **5**, 3127–3148.
45 S. Jiang, K. Y. Win, S. Liu, C. P. Teng, Y. Zheng and M.-Y. Han, *Nanoscale*, 2013, **5**, 3127–3148.
46 L.-L. Li, R. Zhang, L. Yin, K. Zheng, W. Qin, P. R. Selvin and Y. Lu, *Angew. Chem., Int. Ed.*, 2012, **25**, 6225–6229.
47 T. Pellegrino, L. Manna, S. Kudera, T. Liedl, D. Koktysh, A. L. Rogach, S. Keller, J. Rädler, G. Natile and W. J. Parak, *Nano Lett.*, 2004, **4**, 703–707.
48 R. A. Sperling, T. Pellegrino, J. K. Li, W. H. Chang and W. J. Parak, *Adv. Funct. Mater.*, 2006, **16**, 943–948.
49 R. A. Sperling, T. Liedl, S. Duhr, S. Kudera, M. Zanella, C.-A. J. Lin, W. H. Chang, D. Braun and W. J. Parak, *J. Phys. Chem. C*, 2007, **111**, 11552–11559.
50 L. Cheng, C. Wang and Z. Liu, *Nanoscale*, 2013, **5**, 23–37.
51 M. del Barrio, S. de Marcos, V. Cebolla, J. Heiland, S. Wilhelm, T. Hirsch and J. Galbán, *Biosens. Bioelectron.*, 2014, **59**, 14–20.
52 S. Wilhelm, M. del Barrio, J. Heiland, S. F. Himmelstoß, J. Galbán, O. S. Wolfbeis and T. Hirsch, *ACS Appl. Mater. Interfaces*, 2014, **6**, 15427–15433.
53 F. Vetrone, R. Naccache, A. Zamarrón, A. Juarranz de la Fuente, F. Sanz-Rodríguez, L. Martinez Maestro, E. Martín Rodriguez, D. Jaque, J. García Solé and J. A. Capobianco, *ACS Nano*, 2010, **4**, 3254–3258.
54 Y.-F. Wang, L.-D. Sun, J.-W. Xiao, W. Feng, J.-C. Zhou, J. Shen and C.-H. Yan, *Chem. – Eur. J.*, 2012, **18**, 5558–5564.
55 V. Muhr, S. Wilhelm, T. Hirsch and O. S. Wolfbeis, *Acc. Chem. Res.*, 2014, DOI: 10.1021/ar500253g.
56 F. Vetrone, R. Naccache, V. Mahalingam, C. G. Morgan and J. A. Capobianco, *Adv. Funct. Mater.*, 2009, **19**, 2924–2929.
57 U. Resch-Genger, W. Bremser, D. Pfeifer, M. Spieles, A. Hoffmann, P. C. DeRose, J. C. Zwinkels, F. Gauthier, B. Ebert, R. D. Taubert, J. Voigt, J. Hollandt and R. Macdonald, *Anal. Chem.*, 2012, **84**, 3899–3907.

